Invited Feature Article

Tailoring Surface Plasmons through the Morphology and Assembly of Metal Nanoparticles

Luis M. Liz-Marzán*

Departamento de Química Física, Universidade de Vigo, 36310 Vigo, Spain

Received May 19, 2005. In Final Form: July 27, 2005

Metal nanoparticles can be used as building blocks for the formation of nanostructured materials. For the design of materials with specific (optical) properties, several approaches can be followed, even when starting from the very same basic units. In this article, a survey is provided of the optical properties of noble metal nanoparticles, specifically gold, silver, and their combinations, prepared in solution through colloid chemical methods. The optical properties are shown to be mainly influenced by the surface plasmon resonance of conduction electrons, the frequency of which is not only determined by the nature of the metal but also by a number of other parameters, such as particle size and shape, the presence of a capping shell on the particle surface, or the dielectric properties of the surrounding medium. Recent results showing how these various parameters affect the optical properties are reviewed. The results highlight the high degree of control that can now be achieved through colloid chemical synthesis.

Introduction

Research on metal nanoparticles has evolved tremendously since the pioneering work by Michael Faraday in the 19th century[1] and the revitalization, mainly by the groups of Henglein[2] and Kreibig,[3] in the 1980s. Although the initial efforts were directed at identifying and quantifying size effects (relationship between particle size and optical/electronic properties), the development of synthetic techniques, largely deriving from colloid chemistry, has allowed researchers to control various other parameters which affect (often to a larger extent than particle size) the properties of the metals. Such parameters include composition (doping, alloying), surface modification (including deposition of shells, either of another metal, a semiconductor or a dielectric), particle shape, medium refractive index, surface charge, and interparticle interactions.[4] Other methods that have significantly advanced over the past decade come from the refinement of lithographic techniques.[5,6] Of particular relevance in this respect has been the work by Aussenegg,[7−11] Van Duyne,[12−15] and their co-workers, who have characterized various nanometallic geometries and assemblies lithographically grown on solid substrates. This progress in preparation methods has been accompanied by the fast development of more accurate and sophisticated detection techniques, which even allow measurement of the optical signatures of single nanoparticles.[16−21]

There have also been strong advancements in theoretical modeling over the past couple of decades, which have exploited the availability of faster and cheaper computers. Although the standard approaches to light absorption and scattering based on Gustav Mie theory (and modifications thereof)[22] are still largely employed, this model is of limited applicability to current systems, such as coupled particles, and fails to properly reproduce the optical response of systems with increasing geometrical complexity. Consequently, the development of new models which can be applied in a more general fashion has been demanded. Indeed, theoretical work has been carried out, for instance applying the so-called discrete dipole approximation (DDA),[23] in which the particle is divided into small elements interacting with each

* To whom correspondence should be addressed. Tel.: +34 986812298. Fax: +34 986812556. E-mail: lmarzan@uvigo.es.

(1) Faraday, M. *Philos. Trans. Royal Soc. London* **1857**, *147*, 145.
(2) Henglein, A. *Chem. Rev.* **1989**, *89*, 1861.
(3) Kreibig, U. *Z. Phys. D* **1986**, *3*, 239.
(4) Special issue on *Synthesis and Plasmonic Properties of Nanostructures*; *MRS Bull.* **2005**, *30*, issue 5.
(5) Jiang, N.; Hembree, G. G.; Spence, J. C. H.; Qiu, J.; Garcia de Abajo, F. J.; Silcox, J. *Appl. Phys. Lett.* **2003**, *83*, 551.
(6) Kosiorek, A.; Kandulski, W.; Glaczynska, H.; Giersig, M. *Small* **2005**, *1*, 439.
(7) Schider, G.; Krenn, J. R.; Gotschy, W.; Lamprecht, B.; Ditlbacher, H.; Leitner, A.; Aussenegg, F. R. *J. Appl. Phys.* **2001**, *90*, 3825.
(8) Krenn, J. R.; Schider, G.; Rechberger, W.; Lamprecht, B.; Leitner, A.; Aussenegg, F. R.; Weeber, J. C. *Appl. Phys. Lett.* **2000**, *77*, 337.
(9) Krenn, J. R.; Weeber, J. C.; Dereux, A.; Bourillot, E.; Goudonnet, J. P.; Schider, B.; Leitner, A.; Aussenegg, F. R.; Girard, C. *Phys. Rev. B* **1999**, *60*, 5029.
(10) Schaich, W. L.; Schider, G.; Krenn, J. R.; Leitner, A.; Aussenegg, F. R.; Puscasu, I.; Monacelli, B.; Boreman, G. *Appl. Opt.* **2003**, *42*, 5714.
(11) Drezet, A.; Stepanov, A. L.; Ditlbacher, H.; Hohenau, A.; Steinberger, B.; Aussenegg, F. R.; Leitner, A.; Krenn, J. R. *Appl. Phys. Lett.* **2005**, *86*, 074104/1.
(12) Malinsky, M. D.; Kelly, K. L.; Schatz, G. C.; Van Duyne, R. P. *J. Phys. Chem. B* **2001**, *105*, 2343.
(13) Haynes, C. L.; Van Duyne, R. P. *J. Phys. Chem. B* **2001**, *105*, 5599.
(14) Haynes, C. L.; McFarland, A. D.; Smith, M. T.; Hulteen, J. C.; Van Duyne, R. P. *J. Phys. Chem. B* **2002**, *106*, 1898.
(15) Haynes, C. L.; McFarland, A. D.; Zhao, L. L.; Van Duyne, R. P.; Schatz, G. C.; Gunnarsson, L.; Prikulis, J.; Kasemo, B.; Kaell, M. *J. Phys. Chem. B* **2003**, *107*, 7337.
(16) Klar, T.; Perner, M.; Grosse, S.; von Plessen, G.; Spirkl, W.; Feldmann, J. *Phys. Rev. Lett.* **1998**, *80*, 4249.
(17) Emory, S. R.; Haskins, W. E.; Nie, S. *J. Am. Chem. Soc.* **1998**, *120*, 8009.
(18) McCarty, G. S.; Love, J. C.; Kushmerick, J. G.; Charles, L. F.; Keating, C. D.; Toleno, B. J.; Lyn, M. E.; Castleman, A. W., Jr.; Natan, M. J.; Weiss, P. S. *J. Nanoparticle Res.* **1999**, *1*, 459.
(19) Sonnichsen, C.; Geier, S.; Hecker, N. E.; von Plessen, G.; Feldmann, J.; Ditlbacher, H.; Lamprecht, B.; Krenn, J. R.; Aussenegg, F. R.; Chan, V. Z−H.; Spatz, J. P.; Moller, M. *Appl. Phys. Lett.* **2000**, *77*, 2949.
(20) Sonnichsen, C.; Franzl, T.; Wilk, T.; von Plessen, G.; Feldmann, J.; Wilson, O.; Mulvaney, P. *Phys. Rev. Lett.* **2002**, *88*, 077402/1.
(21) Aizpurua, J.; Hanarp, P.; Sutherland, D. S.; Käll, M.; Bryant, G. W.; García de Abajo, F. J. *Phys. Rev. Lett.* **2003**, *90*, 057401/1.
(22) Bohren, C. F.; Huffman, D. F. *Absorption and Scattering of Light by Small Particles*; Wiley: New York, 1983.
(23) Draine, B. T.; Flateau, P. J. *User Guide for the Discrete Dipole Approximation DDSCAT.6.0*; http://arxiv.org/abs/astro-ph0309069.

10.1021/la0513353 CCC: $33.50
Published on Web 08/27/2005

other through dipole−dipole interactions, and subsequently a global evaluation of absorption and scattering is performed. This approximation was initially devised to model scattering and absorption of electromagnetic waves by targets with arbitrary geometries and complex refractive index but has later been successfully implemented for small particles.[24,25]

In this feature article, it was not intended to cover the optical theories in detail, since a good number of excellent reviews have been published on the topic (see references below), and the reader is encouraged to read them for details. Instead, the following section is devoted to explaining the origin of surface plasmons and the relative magnitude of various parameters on the values of plasmon frequency. The subsequent content aims to describe selected results obtained by our group (and colleagues) over the past few years related to the synthesis and processing of various kinds of metal nanoparticles using colloid chemistry methods, with the objective of achieving a high degree of control of the optical response, derived from surface plasmon manipulation. In particular, we start with nanoparticles containing both gold and silver, focusing on the different effects derived from the distribution of the metals (alloys vs core−shells). Then we turn to shape effects, starting with the possibility to modulate the optical response of Au nanorods through nanorod alignment and illumination with polarized light, which in turn serves to introduce various examples of linear assemblies of nanoparticles using carbon nanotubes as templates, showing either isotropic or anisotropic interparticle interactions. Optical effects due to interparticle interactions in multilayer films of Au nanoprisms are discussed in the final section. Through these examples, the current state of the art of this hot topic is outlined, while questions that remain to be answered are left open.

Surface Plasmon Resonance

Optical Effects. Electromagnetic surface waves can propagate along the interface between conducting materials and a dielectric[26] over a broad range of frequencies, ranging from dc and radio frequencies up to the visible. The oscillation modes comprise an electromagnetic field coupled to the oscillations of conduction electrons and are called surface plasmons. They are characterized by strong field enhancement at the interface, while the electric field vector decays exponentially away from the surface (in the nm range).[27−29] When the dimensions of the conductor are reduced, boundary and surface effects become very important, and for this reason, the optical properties of small metal nanoparticles are dominated by such a collective oscillation of conduction electrons in resonance with incident electromagnetic radiation.[30] For many metals such as Pb, In, Hg, Sn, and Cd, the plasma frequency lies in the UV part of the spectrum and nanoparticles do not display strong color effects. Such small metal particles are also readily oxidized making surface plasmon experiments difficult. The coinage elements are exceptional. First they are more noble and form air-stable colloids. Second due to d−d band transitions, the plasma frequency is pushed into the visible part of the spectrum. Hence, surface plasmon experiments are most commonly carried out with Cu, Ag, and Au. In simple terms, the formation of a surface plasmon can be seen as follows: the electric field of the incoming radiation induces the formation

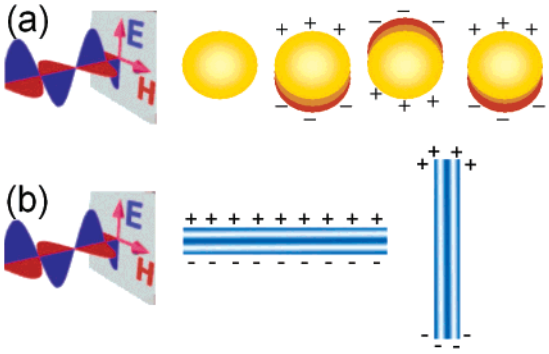

Figure 1. (a) Schematic drawing of the interaction of an electromagnetic radiation with a metal nanosphere. A dipole is induced, which oscillates in phase with the electric field of the incoming light. (b) Transversal and longitudinal oscillation of electrons in a metal nanorod.

of a dipole in the nanoparticle, and there is a restoring force that tries to compensate it, so that a unique resonance frequency matches this electron oscillation within the nanoparticle (see Figures 1a and 2a). Although most interest has focused on size effects, the resonance frequency depends on quite a few additional factors, including particle shape and the nature of the surrounding medium, among others, and their influence is in general larger than that of size. For nonspherical particles, such as rods, the resonance wavelength depends on the orientation of the electric field relative to the particle, and thus, oscillations either along (longitudinal) or across (transversal) the rod are possible[31] (see Figures 1b and 2b). Because of the dimensionality of anisotropic shapes, the frequencies associated with the various resonance modes can be quite different, and thus the optical properties can be largely affected. Since these resonances arise from the particular dielectric properties of the metals, they can be easily modeled using the equations derived by Mie for the resolution of Maxwell equations for the absorption and scattering of electromagnetic radiation by small spheres[32] and their modification by Gans for ellipsoids.[33] Apart from complete descriptions of the theory,[22] the main equations can be found in various recent reviews,[31,34−36] and thus, the reader is referred to them for further details.

The influence of the surrounding medium is usually related to its refractive index,[34] since Mie theory predicts resonance to occur when $\epsilon_1(\omega) = -2\epsilon_m$ ($\epsilon_1(\omega)$ being the real component of the metal dielectric function at angular frequency ω and ϵ_m the medium dielectric constant), but this is only valid for dilute nanoparticle dispersions in nonabsorbing media. However, when concentrated systems are considered, the nanoparticles become closer to each other, and interactions between neighboring particles can arise, so that the models for isolated particles do not hold any longer. The theoretical modeling of concentrated systems requires the use of effective medium theories, such as those derived in the early twentieth century by Maxwell−Garnett[37] and Bruggemann,[38] which allow the calculation of the average dielectric function for composite media with varying concentration of an infiltrated material.

Figure 2 provides an overview of the relative magnitudes of effects that different parameters (particle size, deviation from

(24) Schatz, G. C. *J. Mol. Struct. (THEOCHEM)* **2001**, *573*, 73.
(25) Cao, E.; Schatz, G. C.; Hupp, J. T. *J. Fluoresc.* **2004**, *14*, 331.
(26) Collin, R. *Field Theory of Guided Waves*, 2nd ed.; Wiley: New York, 1990.
(27) Ritchie, R. H. *Phys. Rev.* **1957**, *106*, 874.
(28) Raether, H. *Surface Plasmons*; Springer-Verlag: Berlin, 1988.
(29) Barnes, W. L.; Dereux, A.; Ebbesen, T. W. *Nature* **2003**, *424*, 824.
(30) Kreibig, U.; Vollmer, M. *Optical Properties of Metal Clusters*; Springer-Verlag: Berlin, 1996.
(31) For a full description, see: Pérez-Juste, J.; Pastoriza-Santos, I.; Liz-Marzán, L. M.; Mulvaney, P. *Coord. Chem. Rev.* **2005**, *249*, 1870.
(32) Mie, G. *Ann. Phys.* **1908**, *25*, 377.
(33) Gans, R. *Ann. Phys.* **1912**, *37*, 881.
(34) Mulvaney, P. *Langmuir* **1996**, *12*, 788.
(35) Link, S.; El-Sayed, M. A. *J. Phys. Chem. B* **1999**, *103*, 8410.
(36) Mulvaney, P.; Liz-Marzán, L. M. *Top. Curr. Chem.* **2003**, *226*, 225.
(37) Maxwell Garnett, J. C. *Philos. Trans. R. Soc.* **1904**, *203*, 385. Maxwell Garnett, J. C. *Philos. Trans. R. Soc.* **1906**, *205*, 237.
(38) Bruggeman, D. A. G. *Ann. Phys.* **1935**, *24*, 636.

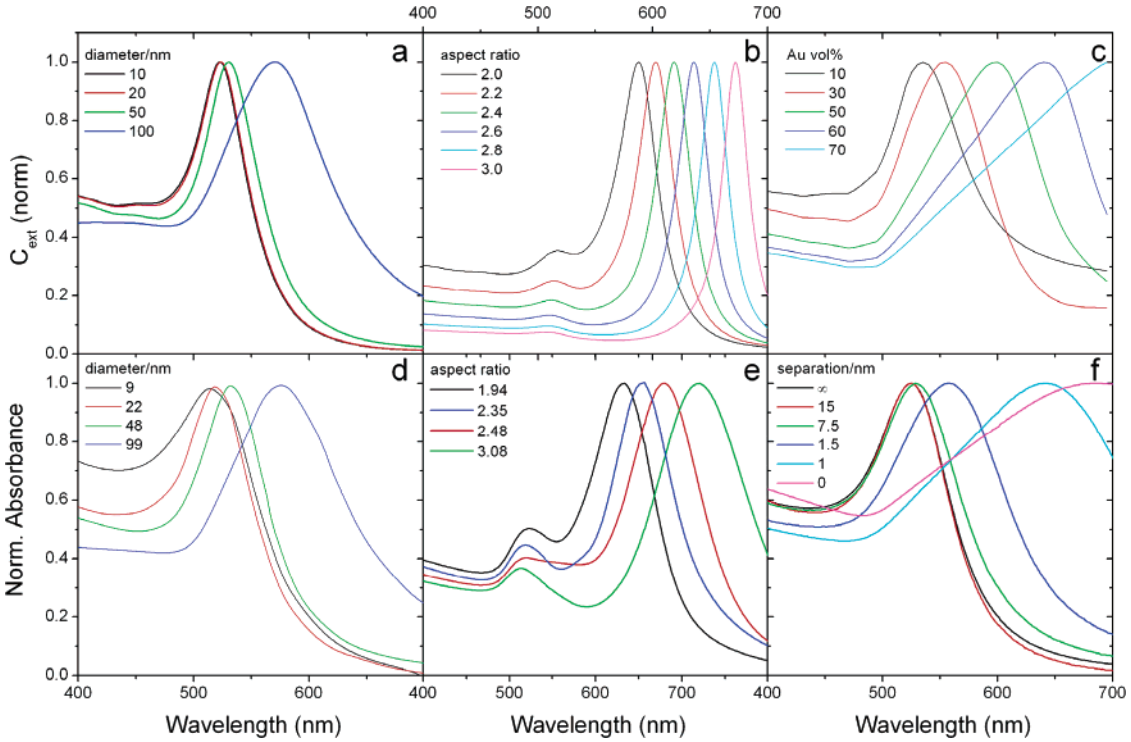

Figure 2. Top: Calculated UV−visible spectra for (a) Au spheres with varying diameters, (b) Au ellipsoids of varying aspect ratio, and (c) thin glass films loaded with increasing Au nanoparticle volume fractions. Bottom: Experimental spectra for (d) Au spheres,[40] (e) Au nanorods, and (f) multilayer films of glass-coated Au spheres with varying interparticle distance.

spherical shape, and interparticle interactions) have on the plasmon resonance frequency (or wavelength, in these plots). All graphs refer to gold, and both calculated and experimental data are shown. Although particle size does influence the position of the surface plasmon band, it is clear from Figure 2 that deviations from spherical geometry are much more relevant. In the calculated spectra shown in Figure 2, it can be seen that, for spherical particles, an increase in diameter from 10 up to 100 nm leads to a red-shift of 47 nm, whereas for prolate ellipsoids, a change in aspect ratio from 2.5 up to 3.5 (implying a much smaller size variation) promotes a red-shift of the longitudinal plasmon band of 92 nm, which is almost double the size effect! Similar effects have been found for other nonspherical geometries through calculations.[24] If we compare Figure 2, panels a and c, we immediately realize that interparticle interactions can also play a fundamental role in the optical absorption of nanoparticle systems. As soon as the nanoparticle volume fraction increases above 10%, the single plasmon band of isolated spheres starts to red-shift and broaden, as a result of dipole−dipole interactions, toward the response expected for a continuous metal film, with high absorption in the IR (free carrier absorption) and the UV (interband transitions) but a small dip in the visible. Similar interparticle interactions have been shown to be responsible for huge field enhancements at Ag nanoparticle junctions, with very important implications on surface enhanced Raman scattering (SERS).[39]

It is important to note that all of these predictions have been confirmed experimentally (Figure 2d−f). Although the agreement is not quantitative, the experimental spectra obtained for aqueous solutions of Au spheres[40] and rods[41] follow the trends predicted by Mie theory, and the same holds for concentrated thin films if we compare the calculations based on Maxwell−Garnett effective medium theory and the results for multilayer thin films where interparticle distance was modulated through the thickness of amorphous silica shells deposited on the Au cores prior to assembly.[42]

So far it has been briefly shown that the degree of control over the optical response from metallic nanostructures has become extremely sophisticated. In what follows, several recent examples of plasmon manipulation are described in detail.

AuAg Bimetallic Nanoparticles

Alloys vs Core−Shells. When nanoparticles are composed of various metals, both the composition and the actual distribution will determine the resulting physicochemical properties, in particular the optical properties. Although various nanoscale bimetallic systems have been studied,[34,43] combinations of gold and silver are particularly interesting, mainly for two reasons: (1) both metals display intense and well-defined surface plasmon absorption bands in the visible (around 400 and 520 nm for spherical nanoparticles of Ag and Au, respectively) and (2) they form fcc crystals with very similar lattice constants (4.078 Å for Au; 4.086 Å for Ag),[44] and for this reason, they can form bulk alloys of any composition. However, either alloying or segregation can be obtained as a result of the combination of both metals within a single nanoparticle. The optical properties of both types of particles have been studied by various groups, and although the results for alloys seem to be in quite good agreement, different interpretations have been published for the properties of core−shell structures. In the case of alloy nanoparticles, normally prepared by simultaneous reduction of the metal salts, several authors[45−49] have shown that there is a linear relationship between

(39) Michaels, A. M.; Jiang, J.; Brus, L. *J. Phys. Chem. B* **2000**, *104*, 11965.
(40) Link, S.; El-Sayed, M. A. *J. Phys. Chem. B* **1999**, *103*, 4212.
(41) Pérez-Juste, J.; Correa-Duarte, M. A.; Liz-Marzán, L. M. *Appl. Surf. Sci.* **2004**, *226*, 137.
(42) Ung, T.; Liz-Marzán, L. M.; Mulvaney, P. *J. Phys. Chem. B* **2001**, *105*, 3441; Ung, T.; Liz-Marzán, L. M.; Mulvaney, P. *Colloid Surf. A* **2002**, *202*, 119.
(43) Liz-Marzán, L. M.; Philipse, A. P. *J. Phys. Chem.* **1995**, *99*, 15120.
(44) Kittel, C. *Introduction to Solid State Physics*; Wiley: New York, 1996.
(45) Papavassiliou, G. C. *Prog. Solid State Chem.* **1980**, *12*, 185.
(46) Han, S. W.; Kim, Y.; Kim, K. *J. Colloid Interface Sci.* **1998**, *208*, 272.

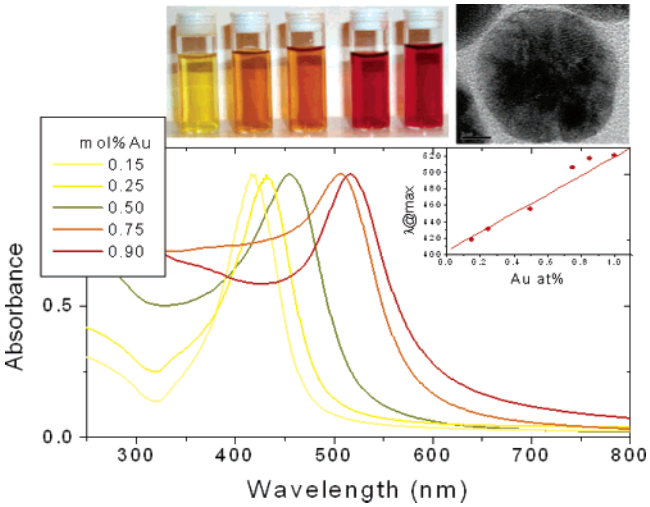

Figure 3. Variation in optical properties (UV−vis spectra and color) for AuAg alloy nanoparticle colloids with varying compositions. In the graph inset, the position of the experimental absorption band (dots) is plotted as a function of composition, and the solid line is a linear fit to values obtained using Mie theory. The HRTEM image shows the homogeneous distribution of Au and Ag atoms within the particles.

the composition of the alloy and the position of the plasmon band, which thus lies between those for pure silver and pure gold nanoparticles, as shown in Figure 3, where photographs of various dispersions confirm a continuous color change between yellow and red as the Au concentration increases. These shifts were initially modeled by assuming a linear combination of the dielectric data of pure gold and silver as input for the Mie calculation, but Link et al.[47] have demonstrated that such calculations lead to incorrect results, and only if the experimental dielectric data for alloy films are used do the predictions agree with the experimental results (see inset plot in Figure 3). Also in Figure 3 a high resolution image is shown of one AuAg alloy particle with 50% molar content of each metal, clearly showing that there is no segregation of the two different metals but rather an intimate mixture, as corresponds to an alloy structure.[50]

Core−shell bimetallic nanoparticles have also been reported by several authors, generated either via segregation during simultaneous reduction or by successive reduction of the different metals. The extensive optical studies on bimetallic nanoparticle colloids performed during the eighties and early nineties are described in the excellent review by Mulvaney[34] and, thus, are not discussed here. However, we shall deal again with the case of core−shells containing gold and silver. The pioneering work by Morriss and Collins[51] was followed by Mulvaney et al.[52] using γ-radiolysis, and later by various groups using successive chemical reduction in solution. Rivas et al.[53] reported both Au@Ag and Ag@Au by citrate reduction, while Srnová-Šloufová et al. used hydroxylamine to grow Au on Ag seeds,[54] and Lu et al. deposited silver shells on citrate stabilized gold nanoparticles using ascorbic acid as a reductant and cetyltrimethylammonium

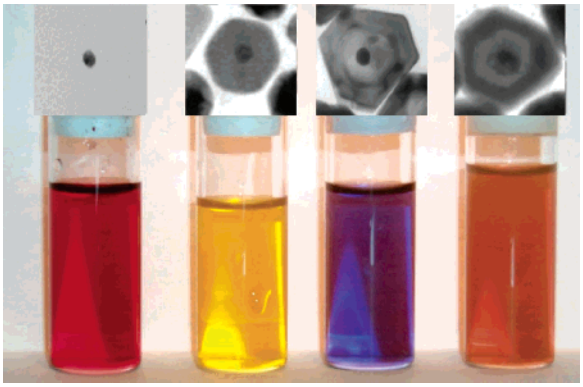

Figure 4. Photographs of aqueous dispersions of (from left to right) Au, Au@Ag, Au@Ag@Au, and Au@Ag@Au@Ag nanoparticles, and the corresponding TEM images. Au core size: 16 nm. Reproduced from ref 64 with permission. Copyright 2005, Royal Society of Chemistry.

chloride (CTAC) as an additional stabilizer during the growth,[55] which yielded quite monodisperse core−shell particles with tunable shell thickness. Interesting optical studies on Au@Ag were also carried out by Kamat and co-workers.[56] Although growth of Ag on Au is not particularly problematic, deposition of Au on Ag is harder to achieve because galvanic displacement can occur, with oxidation of Ag^0 and reduction of Au^{3+} in solution.[57] Actually, this process has been recently exploited by the groups of Xia[58,59] and Mirkin[60] for the creation of complex bimetallic structures in solution. Although deposition of pure Au shells on Ag cores has been claimed,[53,54] the structural characterization of the resulting nanoparticles is not sufficiently clear, and thus modeling of the optical properties is not sufficiently accurate. Following the extensive work of Halas and co-workers on gold[61] and silver[62] nanoshells, Schierhorn and Liz-Marzán[63] produced what is probably the only nanostructure where concentric pure gold and silver layers were produced, using silica as a spacer layer, observing indeed independent absorption by the core and the shell. Unfortunately, both the insulating silica layer and the outer silver shell were too thick to allow a direct comparison with other structures.

Recent experiments[64] showed that successive reduction of $AgNO_3$ and $HAuCl_4$ with ascorbic acid on preformed Au seeds (in the presence of CTAB) can be exploited toward the creation of onion-like multilayer bimetallic nanoparticles, which allows various effects with the same system to be studied. As shown in Figure 4, the color of the dispersion changes dramatically when subsequent metal layers are deposited on the seeds, since the outermost layer is dominating the interaction with incoming light. The TEM images display sufficient contrast to measure the dimensions of the layers, thus allowing comparison of the experimental optical measurements with calculations using a model for multilayer concentric spheres, developed by Quinten[65] on the basis of Mie theory.

(47) Link, S.; Wang, Z. L.; El-Sayed, M. A. *J. Phys. Chem. B* **1999**, *103*, 3529.
(48) Mallin, M. P.; Murphy, C. J. *Nano Lett.* **2002**, *2*, 1235.
(49) Rodríguez-González, B.; Sánchez-Iglesias, A.; Giersig, M.; Liz-Marzán, L. M. *Faradary Discuss* **2004**, *125*, 133.
(50) However, for higher Ag content, the tendency for segregation (of Ag to the nanoparticle surface) has been eventually observed.[49]
(51) Morriss, R. H.; Collins, L. F. *J. Chem. Phys.* **1964**, *41*, 3357.
(52) Mulvaney, P.; Giersig, M.; Henglein, A. *J. Phys. Chem.* **1993**, *97*, 7061.
(53) Rivas, L.; Sánchez-Cortes, S.; García-Ramos, J. V.; Morcillo, G. *Langmuir* **2000**, *16*, 9722.
(54) Srnová-Šloufová, I.; Lednickỳ, F.; Gemperle, A.; Gemperlová, J. *Langmuir* **2000**, *16*, 9928.
(55) Lu, L.; Wang, H.; Zhou, Y.; Xi, S.; Zhang, H.; Hu, J.; Zhao, B. *Chem. Commun.* **2002**, 144.
(56) Kamat, P. V., Flumiani, M.; Dawson, A. *Colloid Surf. A* **2002**, *202*, 269.
(57) Ung, T.; Liz-Marzán, L. M.; Mulvaney, P. *Langmuir* **1998**, *14*, 3740.
(58) Sun, Y.; Xia, Y. *Adv. Mater.* **2004**, *16*, 264.
(59) Sun, Y.; Wiley, B.; Li, Z.-Y.; Xia, Y. *J. Am. Chem. Soc.* **2004**, *126*, 9399.
(60) Sanedrin, R. G.; Georganopoulou, D. G.; Park, S.; Mirkin, C. A. *Adv. Mater.* **2005**, *17*, 1027.
(61) Oldenburg, S.; Averitt, R. D.; Westcott, S.; Halas, N. J. *Chem. Phys. Lett.* **1988**, *288*, 243. Oldenburg, S. J.; Jackson, J. B.; Westcott, S. L.; Halas, N. J. *Appl. Phys. Lett.* **1999**, *75*, 2897. Prodan, E.; Nordlander, P.; Halas, N. J. *Nano Lett.* **2003**, *3*, 1411.
(62) Jackson, J. B.; Halas, N. J. *J. Phys. Chem. B* **2001**, *105*, 2743.
(63) Schierhorn, M.; Liz-Marzán, L. M. *Nano Lett.* **2002**, *2*, 13.
(64) Rodríguez-González, B.; Burrows, A.; Watanabe, M.; Kiely, C. J.; Liz Marzán, L. M. *J. Mater. Chem.* **2005**, *15*, 1755.

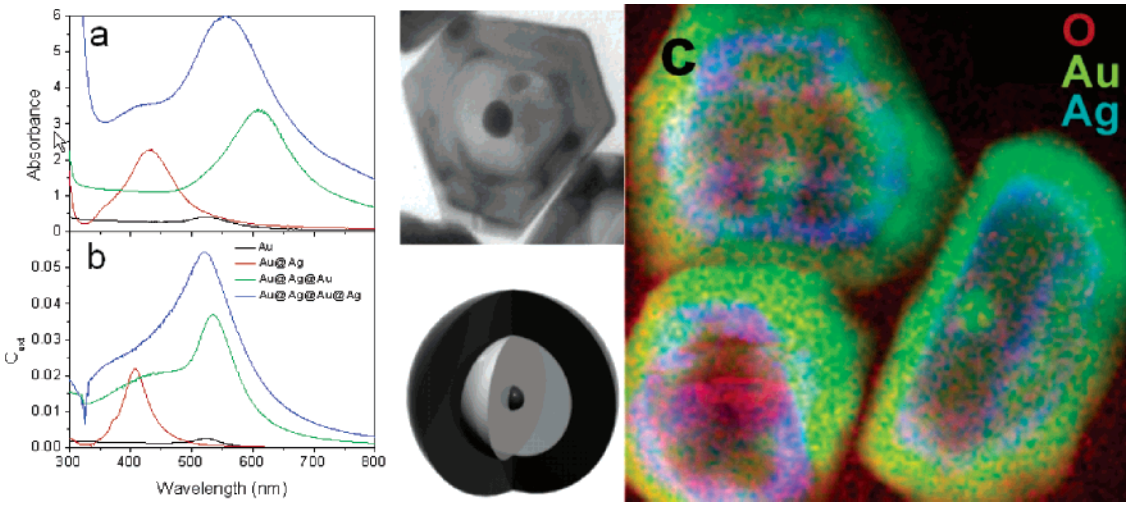

Figure 5. (a) UV−visible spectra of colloids containing Au and AuAg nanoparticles after subsequent reduction/deposition steps. (b) Extinction spectra calculated using Mie theory for multilayer concentric spheres. Average total particle diameters are 17, 49, 82, and 98 nm for Au, Au@Ag, Au@Ag@Au, and Au@Ag@Au@Ag, respectively. (c) RGB image obtained by STEM-XEDS analysis of Au@Ag@Au nanoparticles, showing the relative distribution of the elements (red = O; green = Au; blue = Ag). Adapted from ref 64 with permission. Copyright 2005, Royal Society of Chemistry.

An example is shown in Figure 5 of the comparison between experimental (a) and calculated (b) optical spectra for the subsequent deposition of Ag (16 nm), Au (16.5 nm), and Ag (8 nm) layers on 17 nm Au spheres. Although the calculated spectra closely resemble the experimental ones, there are quantitative differences, especially after the third layer (Au). The reason for this can be a summation of effects, including the deviation from spherical geometry observed in TEM when the Au layer is grown (compare the TEM picture with the drawing in Figure 5), since it has been observed that the presence of sharp edges leads to significant red shifts of the resonance wavelength.[24] On the other hand, a combination of STEM, X-ray spectrum imaging and multivariate statistical analysis (MSA) of the Au@Ag@Au nanoparticles[64] clearly shows that the intermediate Ag layer is preferentially located next to the outer Au shell, as shown in the RGB image (Figure 5c) which reveals the relative spatial distribution of the elements within the particles. A second factor which may explain the deviation from theory is the assumption of well defined shell layers. If the three layers are not well defined, the use of dielectric values within the model may have not been properly used. The observed metal distribution can be either related to galvanic replacement[59] or to interdiffusion of Ag atoms into the Au shell, leading to alloy formation. Other examples of transition from the core−shell to alloy structure were demonstrated by several groups,[66,67] through heating induced by laser irradiation. Additionally, Meisel and co-workers[68] have shown that the stability of the core−shell geometry depends on the particle size, with a complete interdiffusion at room temperature for core sizes below 4.6 nm.

These results suggest that the synthesis of well-defined Ag@Au core−shell nanoparticles requires a tight control of the electrochemical potentials and reduction conditions and can only be trusted after careful space-resolved analysis of the metal distribution within the particles.

Gold Nanorod Alignment and Patterning

One of the most exciting properties of anisotropic metal nanoparticles is their polarization dependent response to incident light. As mentioned in the Introduction, for elongated nanoparticles (such as nanorods), two different resonance modes are possible, as a function of their orientation with respect to the direction of the electric field of incoming electromagnetic radiation (see Figure 1). The resonance parallel to the long axis of the rods determines the longitudinal surface plasmon absorption (SPL) band, whereas the resonance perpendicular to the long axis leads to a transverse surface plasmon absorption (SPT) band, with the SPL band located at lower energies (higher wavelength) and with a much higher absorption coefficient. When metal nanorods are dispersed in a solvent, the random orientation due to the continuous Brownian motion leads to a global absorption spectrum containing both bands, which can be modeled using the modification of Mie theory derived by Gans for prolate ellipsoids.[31,69] Although this model reproduces reasonably well the shape of the spectra, as well as the shifts due to changes in aspect ratio or medium refractive index, there are quantitative deviations from the experimental values that still need to be clarified but can be simply due to the polydispersity of the samples, since single nanorod spectra have been shown to agree reasonably well with the prediction.[20] Still, the model also allows one to calculate the extinction coefficient as a function of polarization angle θ

$$C_{ext} = k\, Im\{\alpha_T(1 - \cos^2(\theta)) + \alpha_L(\cos^2(\theta))\} \qquad (1)$$

Here, α_T and α_L are the polarizabilities of the ellipsoids along the short and long axes, respectively. Thus, if a sufficient number of nanorods could be oriented in the same direction so that enough signal can be collected with a spectrophotometer, use of polarized light should allow this theory to be tested. Similar effects have been observed[70] for chains of silver nanoparticles formed within polyethylene films upon stretching, mainly due to decoupling of unidirectional interaction modes within the chains. After the early work by Foss Jr. et al.[71] using arrays or parallel nanorods directly synthesized in porous membranes, the first exhaustive

(65) Sinzig, J.; Quinten, M. *Appl. Phys. A* **1994**, *58*, 157.
(66) Hodak, J. H.; Henglein, A.; Giersig, M.; Hartland, G. V. *J. Phys. Chem. B* **2000**, *104*, 11708.
(67) Abid, J.-P.; Girault, H. H.; Brevet, P. F. *Chem. Commun.* **2001**, 829.
(68) Shibata, T.; Bunker, B. A.; Zhang, Z.; Meisel, D.; Vardeman, C. F., II.; Gezelter, J. D. *J. Am. Chem. Soc.* **2002**, *124*, 11989.
(69) Gans, R. *Ann. Phys.* **1912**, *37*, 881.
(70) Dirix, Y.; Bastiaansen, C.; Caseri, W.; Smith, P. *Adv. Mater.* **1999**, *11*, 223.
(71) Foss, C. A., Jr.; Hornyak, G. L.; Stockert, J. A.; Martin, C. R. *J. Phys. Chem.* **1994**, *98*, 2963.

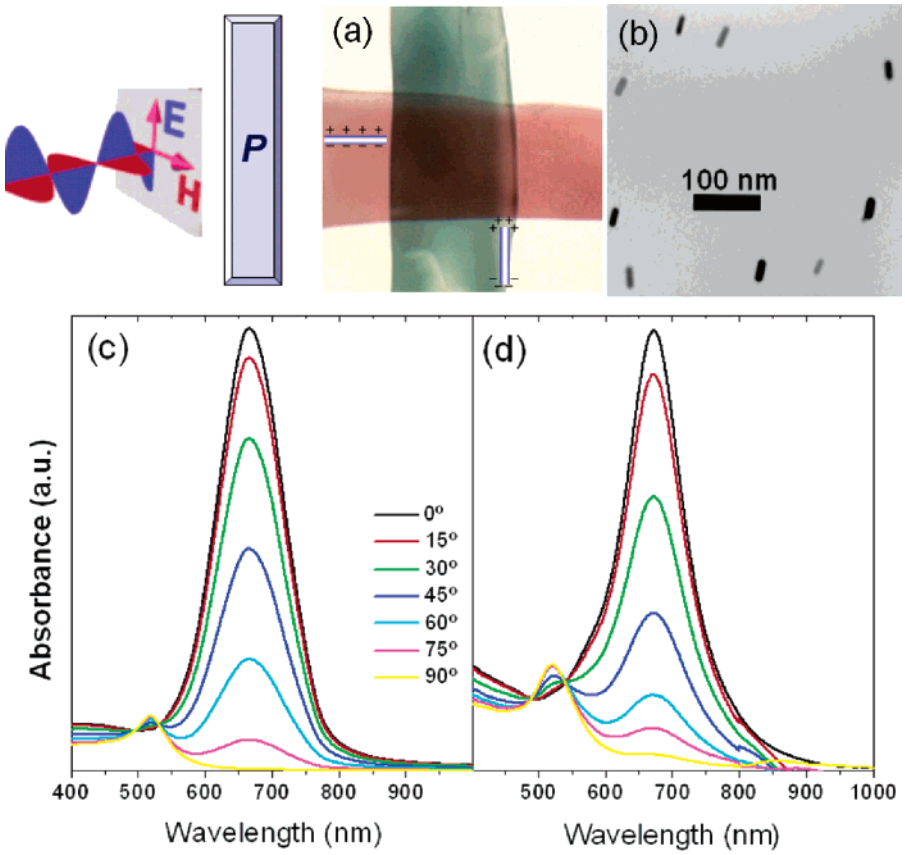

Figure 6. (a) Photograph of PVA films containing Au nanorods aligned parallel (blue film) and perpendicular (red film) to the electric field of polarized incoming light. (b) TEM image showing the preferential alignment of nanorods in a stretched PVA film. (c) Calculated and (d) experimental UV−vis−NIR spectra of PVA films containing aligned Au nanorods (aspect ratio 2.23) for varying polarization angles as indicated. c: For the calculation, a matrix with refractive index 1.5 and rods with an aspect ratio of 2.3±0.6 were used. Adapted from ref 75 with permission. Copyright 2005, Wiley-VCH.

polarization experiments on nanorods were performed by van der Zande et al.[72] using Au nanorods synthesized by electrochemical growth within alumina membranes. The alignment of the nanorods was achieved both using electric fields in aqueous solution and by stretching poly(vinyl alcohol) (PVA) films containing the nanorods.[73] Similar experiments were later carried out by Wilson et al. using silver nanorods.[74] A refinement of this latter procedure has been recently reported by Pérez-Juste et al.[75] using more monodisperse nanorods prepared by the seeded growth method, initially developed by Murphy and co-workers[76−78] and later modified by Nikoobakht and El-Sayed.[79] Photographs of crossed PVA films with oriented Au nanorods showing the different colors when illuminated by polarized light are shown in Figure 6 (upper panel), together with a representative TEM image showing the preferential alignment of the nanorods upon stretching of the film. As predicted by eq 1, the contribution of both plasmon resonances varies gradually when the polarization angle of the incident light is varied from 0° to 90°, which is reflected in the two isosbestic points observed in both the experimental and calculated spectra shown in the lower panel of Figure 6. The calculated spectra were obtained taking into account the sample polydispersity, and an average aspect ratio of 2.3±0.6 nm was found to reproduce the experimental spectra. As a result of the polydispersity, the SPL band is red-shifted with respect to the values for monodisperse nanorods because of the larger absorption coefficient of longer rods.

The different optical response of Au nanorods and nanospheres, coupled to the reported thermal reshaping of Au nanorods into spheres through laser irradiation,[80,81] offer a unique possibility to create well-defined patterns on polymer films loaded with oriented metal nanorods. A first example was shown by Wilson et al.,[74] where Ag nanorod-PVA composite films were irradiated with a 355 nm Nd:YAG nanosecond laser. Although only a relatively large pattern was "drawn" in that work, it was recently demonstrated[75] that much smaller features can be reproduced on Au nanorod-PVA films using a ns laser tuned at 1064 nm. The high intensity of the pulse was sufficient to convert the gold rods into spheres, whereas the short duration does not allow the diffusion of a high amount of energy as heat to the polymer matrix, and therefore, this is not deformed during the process. The effects of irradiation when a 100 mesh copper TEM grid was used as a template (partially blocking the laser beam path) are shown in Figure 7. The grid pattern has been perfectly reproduced on the film, including small defects, and is observed in Figure 7a as red (irradiated) and blue (nonirradiated) areas. This color contrast stems from the reshaping of rods into spheres,

(72) van der Zande, B. M. I.; Koper, G. J. M.; Lekkerkerker, H. N. W. *J. Phys. Chem. B* **1999**, *103*, 5754.
(73) van der Zande, B. M. I.; Pagès, L.; Hikmet, R. A. M.; van Blaaderen, A. *J. Phys. Chem. B* **1999**, *103*, 5761.
(74) Wilson, O.; Wilson, G. J.; Mulvaney, P. *Adv. Mater.* **2002**, *14*, 1000.
(75) Pérez-Juste, J.; Rodríguez-González, B.; Mulvaney, P.; Liz-Marzán, L. M. *Adv. Funct. Mater.* **2005**, *15*, 1065.
(76) Jana, N. R.; Gearheart, L.; Murphy, C. J. *Chem. Mater.* **2001**, *13*, 2313.
(77) Jana, N. R.; Gearheart, L.; Murphy, C. J. *Langmuir* **2001**, *17*, 6782.
(78) Jana, N. R.; Gearheart, L.; Murphy, C. J. *J. Phys. Chem. B* **2001**, *105*, 4065.
(79) Nikoobakht, B.; El-Sayed, M. A. *Chem. Mater.* **2003**, *15*, 1957.
(80) Chang, S.-S.; Shih, C.-W.; Chen, C.-D.; Lai, W.-C.; Wang, C. R. C. *Langmuir* **1999**, *15*, 701.
(81) Link, S.; Burda, C.; Nikoobakht, B.; El-Sayed, M. A. *Chem. Phys. Lett.* **1999**, *315*, 12.

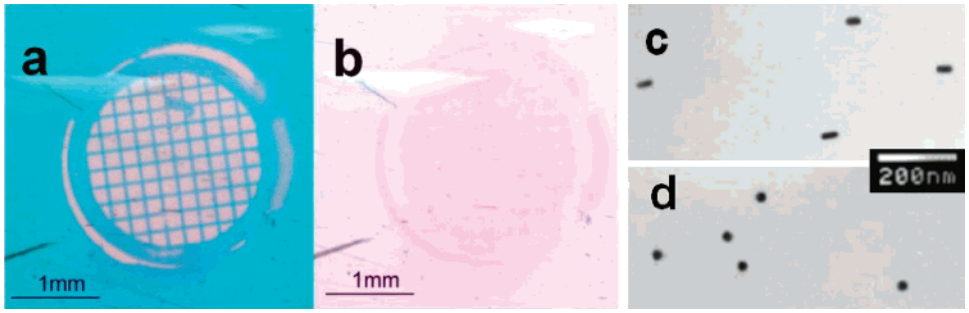

Figure 7. (a and b) Photographs of a PVA film containing aligned Au nanorods (a.r. 2.23), irradiated with a single pulse of a ns laser using a TEM grid as a mask, illuminated under parallel (a) and perpendicular (b) polarization. (c and d) Transmission electron micrographs of PVA films containing aligned Au nanorods (aspect ratio: 2.23) before (a) and after (b) irradiation with a ns laser. Adapted from ref 75 with permission. Copyright 2005, Wiley-VCH.

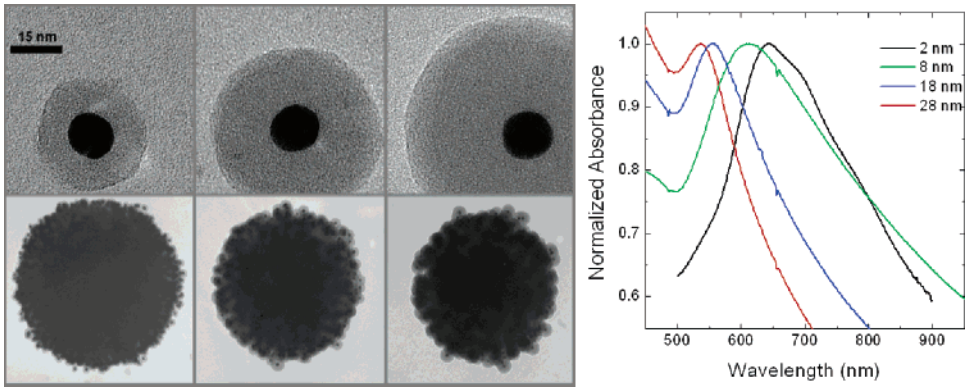

Figure 8. Left: TEM micrographs of $Au@SiO_2$ nanoparticles with 13 nm Au cores and varying shell thicknesses (8, 18, and 28 nm), and the same particles assembled on 640 nm PS spheres. Right: Normalized UV−visible spectra of dilute dispersions of 640 nm PS spheres coated with five monolayers of $Au@SiO_2$ nanoparticles (silica shell thickness is indicated in the labels). Adapted from ref 90b.

as demonstrated in the TEM images of Figure 7c,d. Interestingly, the contrast between irradiated and nonirradiated areas changes enormously when the polarization angle is varied from 0° (Figure 7a) to 90° (Figure 7b), since the single absorption band of the spheres almost coincides with the transverse plasmon band of the rods (selectively excited at 90°). Higher magnification images of the same film demonstrate that there is no physical damage to the polymer matrix, and the lines separating red and blue areas are extremely well defined, which suggests a very fine resolution in this printing technique. Actually, TEM observation at the border shows even partially deformed nanorods.[75]

Since the optical manipulation of polymer−nanorod composites has been clearly demonstrated, an obvious development should come from the use of elastomers as substrates, so that reversible alignment of the nanorods can be achieved. Additionally, the possibility of printing even smaller features than the ones shown in Figure 7 still needs to be tested and may be limited both by the actual size of the rods and separation between them and by the wavelength of the laser beam.

Isotropic vs Anisotropic Colloidal Assemblies

Focus over the last five years has shifted form the preparation of anisotropic nanoparticles toward their assembly into functional structures: nanoassemblies. In particular, linear nanoarrays based on metal nanoparticles[82−84] offer a huge potential for applications not only in microelectronics[85] but also in photonics, since the use of metal nanoparticle chains for wave guiding via surface plasmons has been predicted.[86,87] For such applications, it is important not only to be able to manipulate the particles on the nanoscale but also to characterize interparticle interactions. In the case of metal nanoparticles, such interactions arise mainly because of the coupling of plasmon modes if the distance between particles is small enough. Several studies have been performed on plasmon coupling for gold nanoparticle thin films on solid substrates, using either organic ligands[88,89] or inorganic (silica) shells[42] as spacers. As shown in Figure 2, although continuous gold films (nanoparticles in contact with each other) display absorption in the whole visible range, with a dip at ca. 475 nm, as the separation distance increases, a well defined band arises at high wavelengths and steadily blue-shifts and gets narrower until, for a separation on the order of two particle diameters, the spectrum basically coincides with that of individual, infinitely separated nanoparticles (see Figure 2c,f). Similar effects have been observed when the assembly of silica-coated gold ($Au@SiO_2$) nanoparticles is performed on colloidal substrates (polystyrene spheres);[90] that is, composite colloids containing $Au@SiO_2$ with thick shells show "single-particle" plasmon bands, whereas the plasmon band for those with thin shells is broader and red-shifted. Examples of nanostructured colloids formed by assembly on 640 nm polystyrene (PS) spheres of $Au@SiO_2$ with identical cores but silica shells with various thickness are shown in Figure 8. It is clear that, although the outer surface is rough,

(82) Novak, J. P.; Feldheim, D. L. *J. Am. Chem. Soc.* **2000**, *122*, 3979.
(83) Chandrasekharan, N.; Kamat, P. V. *Nano Lett.* **2001**, *1*, 67.
(84) Hassenkam, T.; Nørgaard, K.; Iversen, L.; Kiely, C. J.; Brust, M.; Bjørnholm, T. *Adv. Mater.* **2002**, *14*, 1126.
(85) Park, S. J.; Taton, T. A.; Mirkin, C. A. *Science* **2002**, *295*, 1503.
(86) Quinten, M.; Leitner, A.; Krenn, J. R.; Aussenegg, F. R. *Opt. Lett.* **1998**, *23*, 1331.
(87) Panoiu, N.-C.; Osgood, R. M., Jr. *Nano Lett.* **2004**, *4*, 2427.
(88) Brust, M.; Bethell, D.; Kiely, C. J.; Schiffrin, D. J. *Langmuir* **1998**, *14*, 5425.
(89) Chumanov, G.; Sokolov, K.; Cotton, T. M. *J. Phys. Chem.* **1996**, *100*, 5166. Malynych, S.; Chumanov, G. *J. Am. Chem. Soc.* **2003**, *125*, 2896.
(90) Caruso, F.; Spasova, M.; Salgueiriño-Maceira, V.; Liz-Marzán, L. M. *Adv. Mater.* **2001**, *13*, 1090. Salgueiriño-Maceira, V.; Caruso, F.; Liz-Marzán, L. M. *J. Phys. Chem. B* **2003**, *107*, 10990.

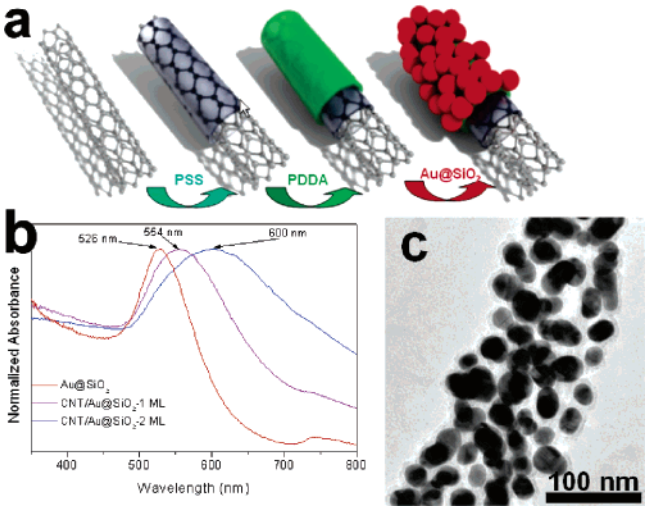

Figure 9. (a) Schematic drawing of nanoparticle assembly on CNTs, involving polymer wrapping followed by layer-by-layer assembly. (b) Normalized UV−vis spectra of aqueous dispersions of CNTs (15 nm outer diameter) after LBL assembly of 1 and 2 monolayers of $Au@SiO_2$ nanoparticles (16 nm core diameter, 2 nm shell thickness). The spectrum of the precursor $Au@SiO_2$ colloid is shown as a reference. (c) TEM micrograph of a MWNT (15 nm diameter) on which 1 monolayer of $Au@SiO_2$ nanoparticles was assembled. Adapted from ref 91 with permission. Copyright 2004, Wiley-VCH.

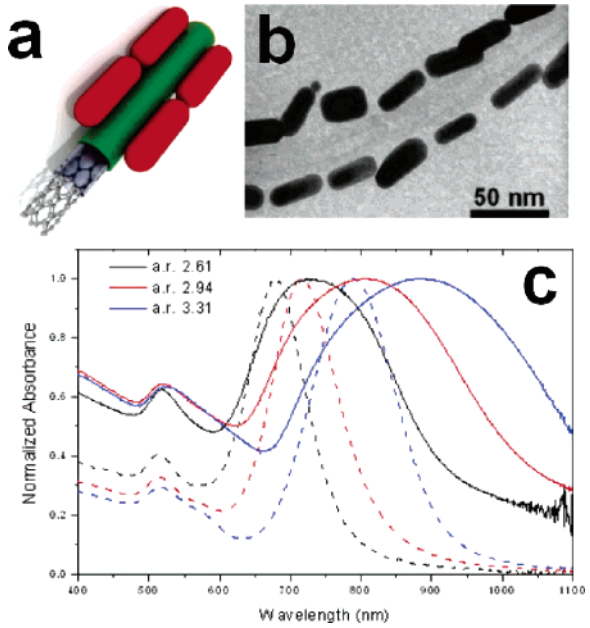

Figure 10. (a and b) Drawing and TEM micrograph of a selected area of a Au nanorod-MWNT composite; (c) UV−vis spectra of aqueous dispersions of individual Au nanorods (dashed lines) and nanorods attached on MWNTs (solid lines). Average aspect ratios of the nanorods are indicated. Adapted from ref 95 with permission. Copyright 2005, Wiley-VCH.

the coating layers are compact and uniform, so that, the interparticle separation is dictated by the corresponding thickness of the silica shell. UV−visible spectra of PS colloids coated with five monolayers of $Au@SiO_2$ nanoparticles of various shell thickness are also shown in the figure. For thicker silica shells (increased separation between gold cores), the plasmon band is close to that of the initial, isolated Au nanoparticles. Due to the increase in particle size, there is also an increased scattering contribution as more monolayers are deposited, which is reflected in the dramatic increase of the low-wavelength tail of the spectra. These scattering effects also slightly affect the actual position of the plasmon band, as demonstrated by a larger shift as the size of the polystyrene cores is increased.[90]

Recently, experiments have been carried out which can be considered as an extension of this work. Using elongated substrates, in particular carbon nanotubes (CNTs), elongated assemblies were created.[91] On the basis of the electrostatic layer-by-layer (LBL) assembly,[92] polyelectrolytes were used to drive the homogeneous assembly of $Au@SiO_2$ nanoparticles on multiwall CNTs. The hydrophobic nature of the CNTs drives the initial wrapping with a negatively charged polyelectrolyte[93] (poly(sodium 4-styrenesulfonate), PSS), which then provides the necessary negative surface charge for a subsequent layer of positive poly(diallyldimethylammonium chloride) (PDDA), on which the negatively charged nanoparticles can assemble as densely packed monolayers. A schematic drawing of the process as well as the optical effects and a representative TEM image of the composite nanotubes are shown in Figure 9. Similar to the spherical assemblies, the spectra show broadening and red-shift of the plasmon band after one monolayer is assembled on the CNTs. Deposition of a second monolayer leads to a further broadening and red-shift, because of interaction between layers.[42] According to the predictions by Panoiu and Osgood,[75] and the experimental results of Dirix et al.[70] from aligned arrays of silver nanoparticles in polymer matrixes, the obtained broad bands should have a longitudinal and a transverse component, which has been observed through alignment of CNTs wrapped with bare Au nanospheres within PVA films.[94]

Even more striking is the optical response of Au nanorod−CNT composites. It has been observed[95] that when gold nanorods capped with PVP (negative surface charge) are assembled on PSS/PDDA coated multiwall CNTs, they do not form a compact, random monolayer like the $Au@SiO_2$ nanoparticles, but rather tend to align in parallel stripes along opposite sides of the CNTs (see scheme and TEM in Figure 10a,b). Although similar head-to-tail assembly of gold nanorods has been previously observed in other systems,[96,97] the reason for this preferential alignment is not perfectly clear but may have to do with the anisotropic surface potential of the nanorods, which has been proposed as the driving force for anisotropic nanoparticle growth.[98] Not only is the morphology of these composite nanostructures interesting but also their optical features. As shown in Figure 10c for experiments performed using nanorods with three different aspect ratios, upon assembly on the CNTs, the longitudinal plasmon band consistently red-shifts and broadens, with a larger effect for longer rods. Meanwhile, the position of the transverse plasmon band remains almost unchanged, which means that we have a selective coupling of the longitudinal modes of neighboring rods. This effect agrees with the observation made by Kamat and

(91) Correa-Duarte, M. A.; Sobal, N.; Liz-Marzán, L. M.; Giersig, M. *Adv. Mater.* **2004**, *16*, 2179.
(92) Kotov, N. A.; Dekany, I.; Fendler, J. H. *J. Phys. Chem.* **1995**, *99*, 13065. Caruso, F.; Caruso, R. A.; Möhwald, H. *Science* **1998**, *282*, 1111.
(93) O'Connel, M. J.; Boul, P.; Ericson, L. M.; Huffman, C.; Wang, Y.; Haroz, E.; Kuper, C.; Tour, J.; Ausman, K. D.; Smalley, R. E. *Chem. Phys. Lett.* **2001**, *342*, 265.
(94) Correa-Duarte, M. A.; Liz-Marzán, L. M., manuscript in preparation.
(95) Correa-Duarte, M. A.; Pérez-Juste, J.; Sánchez-Iglesias, A.; Giersig, M.; Liz-Marzán, L. M. *Angew. Chem. Int. Ed.* **2005**, *44*, 4375.
(96) Caswell, K. K.; Wilson, J. N.; Bunz, U. H. F.; Murphy, C. J. *J. Am. Chem. Soc.* **2003**, *125*, 13914.
(97) Thomas, K. G.; Barazzouk, S.; Ipe, B. I.; Joseph, S. T. S.; Kamat, P. V. *J. Phys. Chem. B* **2004**, *108*, 13066.
(98) Pérez-Juste, J.; Liz-Marzán, L. M.; Carnie, S.; Chan, D. Y. C.; Mulvaney, P. *Adv. Funct. Mater.* **2004**, *14*, 57.

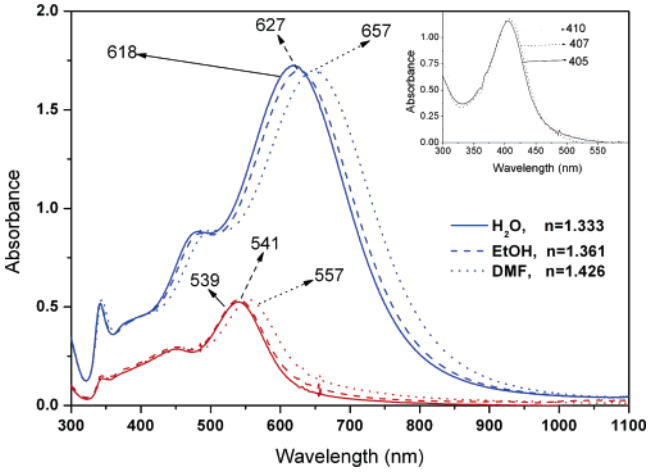

Figure 11. UV−visible spectra of Ag nanosprisms with average lateral dimensions of 80 (blue) and 60 (red) nm, in DMF (dotted lines), ethanol (dashed lines), and water (solid lines). The maximum positions of the in-plane dipole resonance bands are indicated for each solvent. The inset shows the respective spectra for small Ag nanospheres. Adapted from refs 103 and 105.

co-workers during the head-to-tail assembly of similar nanorods using mercaptopropionic acid as a linker molecule.[97] The nanorod−nanotube composites can also be incorporated within PVA films and the polarization-dependent optical response used as a sensor for the alignment of the whole assembly.[95]

It remains to be demonstrated that the described nanostructured materials can be actually used for wave guiding, which may require an even tighter control and manipulation at the nanoscale.

Metal Nanoprisms: Colloids and Assemblies

Another interesting type of metal nanoparticle that has recently acquired attention are nanoprisms, which again can display a wide range of optical features, as a function of shape, lateral size, and thickness.[99] Although triangular and polygonal flat nanoprisms are often obtained during metal colloid preparation, the synthesis of metal flat nanoprisms with relatively high yield is quite recent. Silver nanoprisms have been synthesized in relatively high yields mainly through photochemically induced aggregation of small spheres[100−102] or thermal reduction in organic solvents.[103,104] The optical spectra of such silver nanoprisms (Figure 11) display bands for in-plane dipole resonance, as well as for in-plane and out-of-plane quadrupole resonances, whereas the out-of-plane dipole peak is usually only evident as a small shoulder. Although there is no analytical solution for the plasmon mode energies of such objects, numerical solutions can be obtained by means of the so-called discrete-dipole approximation (DDA).[100]

Apart from the sensitivity toward the actual geometry, it is quite remarkable how sensitive the optical properties of this system are toward refractive index changes in the surrounding medium. A clear demonstration is shown in Figure 11 for Ag nanoparticles prepared by reduction in boiling *N*,*N*-dimethylformamide (DMF) using poly(vinylpyrrolidone) (PVP) as a stabilizer. Although solvent exchange of PVP-protected silver nanospheres (inset) from DMF (n=1.426) to water (n=1.333)

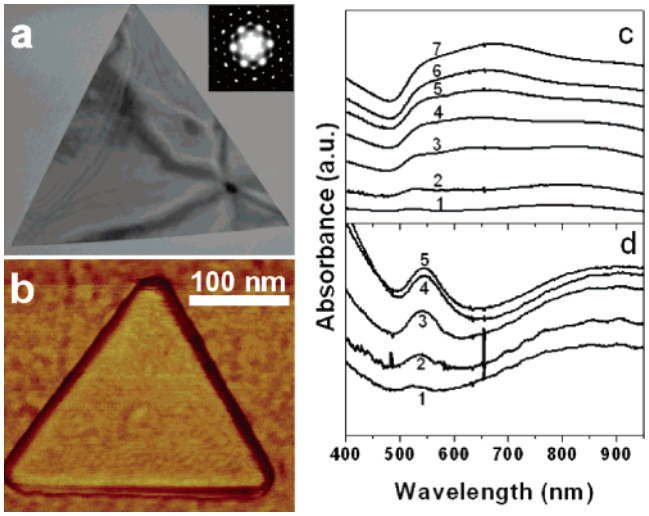

Figure 12. Left: TEM (a) and AFM (b) images showing the flat nature of the Au triangular nanosprisms prepared by reduction with salicylic acid. The inset in (a) is an electron diffraction pattern demonstrating their single-crystal nature. Right: UV−visible spectra of sequentially deposited $(PDDA/Au)_n$, $n = 1-7$ (c) and $(PDDA/Au/PDDA/clay)_n$, $n = 1-5$ films (d). Adapted from ref 107.

leads to a 5 nm blue-shift of the plasmon band,[105] when a similar experiment is performed on a dispersion of nanoprisms with average lateral dimensions of 60 and 80 nm, the in-plane dipole plasmon bands blue-shift almost 20 and 40 nm, respectively, whereas the out-of-plane quadrupole peak remains almost at the same position. This means that the plasmon oscillation in the plane is extremely sensitive to environmental changes, and for this reason, silver nanoprisms can be envisaged as suitable substrates for sensing applications.[106]

Although some procedures have been published for the production of gold nanoprisms,[107−110] optical studies are still rather rare.[107,110] In the previous section, we have seen that interparticle interaction usually leads to a red-shift and broadening of the plasmon absorption band. In the case of spheres, the single resonance band is affected, whereas for nanorods, selective broadening of the longitudinal plasmon band is observed when the rods are assembled in a head-to-tail fashion. The assembly of nanoprisms is also expected to lead to interactions, which should also depend on the actual morphology of the assembly. Such effects have been recently reported by Malikova et al.,[107] using gold nanoprisms, prepared by reduction of $HAuCl_4$ with salicylic acid in water at 80 °C. The TEM and AFM images in Figure 12 clearly demonstrate the flat geometry of the triangular nanoprisms. However, this synthetic procedure also yields a relatively large amount of similarly sized spheres, and separation of the two types of particles is impractical, and for this reason, the optical spectrum of the colloid shows two distinct plasmon bands, one centered at 535 nm due to the dipole resonance of the spheres and another at 840 nm corresponding to the in-plane resonance of the nanoprisms. Due to the polydispersity, the low-energy band is rather broad. The stabilizing layer of salicylic acid renders the particles negatively charged, and thus layer-

(99) Kelly, K. L.; Coronado, E.; Zhao, L. L.; Schatz, G. C. *J. Phys. Chem. B* **2003**, *107*, 668.
(100) Jin, R.; Cao, Y.; Mirkin, C. A.; Kelly, K. L.; Schatz, G. C.; Zheng, J. G. *Science* **2001**, *294*, 1901.
(101) Jin, R.; Cao, Y. C.; Hao, E.; Metraux, G. S.; Schatz, G. C.; Mirkin, C. A. *Nature* **2003**, *425*, 487.
(102) Callegari, A.; Tonti, D.; Chergui, M. *Nano Lett.* **2003**, *3*, 1565.
(103) Pastoriza-Santos, I.; Liz-Marzán, L. M. *Nano Lett.* **2002**, *2*, 903.
(104) Sun, Y.; Xia, Y. *Adv. Mater.* **2003**, *15*, 695.
(105) Pastoriza-Santos, I.; Liz-Marzán, L. M. *Langmuir* **2002**, *18*, 2888.
(106) Haes A. J.; Stuart D. A.; Nie S.; Van Duyne R. P. *J. Fluoresc.* **2004**, *14*, 355.
(107) Malikova, N.; Pastoriza-Santos, I.; Schierhorn, M.; Kotov, N. A.; Liz-Marzán, L. M. *Langmuir* **2002**, *18*, 3694.
(108) Kim, F.; Connor, S.; Song, H.; Kuykendall, T.; Yang, P. *Angew. Chem., Int. Ed.* **2004**, *43*, 3673−3677.
(109) Shankar, S. S.; Rai, A.; Ankamwar, B.; Singh, A.; Ahmad, A.; Sastry, M. *Nature Mater.* **2004**, *3*, 482.
(110) Millstone, J. E.; Park, S.; Shuford, K. L.; Qin, L.; Schatz, G. C.; Mirkin, C. A. *J. Am. Chem. Soc.* **2005**, *127*, 5312.

by-layer assembly can be carried out using a positively charged polyelectrolyte, PDDA.

AFM analysis of the deposited monolayers showed that the polygons lay parallel to the substrate, embedded in a compact monolayer of the spherical nanoparticles. Upon multilayer assembly, a homogeneous increase in the absorbance spectrum was observed as successive monolayers were deposited (see Figure 12a,b). However, although the first deposited gold monolayer displayed absorption bands very similar to those of the starting nanoparticle dispersion, a new optical feature (a band at intermediate energy) progressively developed for subsequent deposited layers, becoming clearly visible in the fourth layer and becoming dominant by the seventh bilayer. This new band at 650 nm is very likely due to interactions between spherical nanoparticles within neighboring layers but also with the nanoprisms. In the latter case, the coupling strength should be higher than in the former because the geometry of sphere on a plane results in greater integral electrostatic attraction than that between two spheres. The variety of different geometrical arrangements causes band broadening, which can also be seen in Figure 12c. Interestingly, when insulating layers made from montmorillonite clay platelets were inserted between every two subsequent metal particle layers (see optical spectra in Figure 12d), the positions of the two original bands of the dispersion remain basically unaltered, as a result of insulation of the adjacent gold nanoparticle layers. In this case, the only optical effect is a slight red-shift due to the refractive index increase after the deposition of the montmorillonite sheets.

Considering the recent progress in the synthesis of gold and silver nanoprisms,[110] it is to be expected that more accurate and clean experiments of this kind will be soon reported. We should also expect detailed studies of the angular dependence of the optical response for nanoprism assemblies, since they typically lie flat on the surface, and thus when varying the incident angle, selective excitation of the in-plane and out-of-plane modes can in principle be achieved. Single-particle spectroscopy can also surely contribute to such studies.

Conclusions

The optical properties of metal nanoparticle systems can be tuned over a wide spectral range through manipulation of various parameters that allow one to tailor surface plasmon resonance frequencies. The effects of nanoparticle composition, shape, orientation, and interparticle interactions have been discussed in the light of recent results for nanoparticles made of gold and silver. It seems clear that the development of colloid chemistry methods continues to be essential for the synthesis and manipulation of such metallic nanostructures, and it is envisaged that during the present decade both the experimental techniques and the modeling will be developed far enough to allow for the following step, i.e., the fabrication of devices that can exploit the fascinating properties of these systems.

Acknowledgment. The author is grateful to many group members and collaborators from other groups who have actively contributed to carry out the research described in this article. Dr. M. A. Correa-Duarte is thanked for assistance in preparation of some figures and Dr. I. Pastoriza-Santos and Prof. P. Mulvaney for critical reading of the manuscript. Financial support from the European Union and the Spanish Ministerio de Educación y Ciencia and Xunta de Galicia are acknowledged.

LA0513353